Imprinted Electrodes for Enhanced Light Trapping in Solution Processed Solar Cells

*Agustín Mihi, Fiona J. Beck, Tania Lasanta, Arup K. Rath, and Gerasimos Konstantatos**

Thin film solar cell technologies are expected to meet several demands including high efficiency, low-cost large-area manufacturability, flexibility, and aesthetic appeal. Solution processed organic and nanocrystal/QD- based solar cells are the most promising candidates in fulfilling these requirements.[1–5] One of the major roadblocks of these material platforms towards higher efficiencies is the low carrier mobility which imposes limits on the thickness of the solar cells to facilitate concurrently high optical absorption and efficient carrier extraction. It is therefore necessary to include a light harvesting scheme that provides light trapping in thin films. Light trapping has always been an important part of the design of the solar cell, maximizing the optical path of light in the device at wavelengths where the absorption coefficient of the active layer is low.[6] Traditional light trapping schemes such as textured surfaces rely on geometrical optics to confine light within wafer-based solar cells, several orders of magnitude thicker than the wavelength of incident light. For thin film solar cells, light needs to be captured within active layers a few hundreds of nanometers thick, a problem that gave rise to a new generation of light trapping schemes:[7,8] Photonic crystals, plasmonic structures, microresonators, and other architectures produce intense localized electromagnetic fields that can enhance the light harvesting efficiency of the active layer.[9–12] In particular, the use of diffractive elements such as 2D periodic arrays has been of great interest in the field proven by the many studies that can be found in the literature.[13–17] However, the manufacturing requisites of low-temperature and large area processing for the photovoltaic devices must also apply to the light trapping schemes.[18] Furthermore, the integration of light trapping structures should not come at the expense of the electrical performance of the cell.

Amongst the different solution processed thin film PV, colloidal quantum dot solar cells make a rapidly developing technology, recently reaching a record efficiency of 7%, based on PbS QDs and titania n-type electrodes.[19] This technology is an ideal candidate to test the functionality and viability of our imprinted electrodes. Among the wide variety of available configurations,[20] we employed the PbS-ZnO heterojunction for it provides efficient devices processed at temperatures lower than 200 °C, suitable for roll-to-roll manufacturing on flexible substrates. Record efficiencies for PbS QDs-ZnO bilayers reported in literature range from 4.4% (using a nanocrystalline ZnO electrode)[21,22] up to 4.9% (using ZnO nanowires).[23]

Here we present an inexpensive light trapping scheme that can be easily integrated in thin film solar cells by substituting the flat TCO substrate (transparent conductive oxide), required in almost all new technologies for an imprinted electrode, capable of both diffracting light and collecting the photogenerated carriers. Indium Tin Oxide (ITO) coated 2D cylindrical hole arrays are fabricated by sputtering the conductive oxide onto a soft imprinted epoxy. The performance of such photonic architectures is tested by fabricating a solution processed solar cell (PbS quantum dots (QDs) – ZnO heterojunction) on these substrates. A power conversion efficiency enhancement of 17.5% was measured for the optimized design compared to traditional flat TCO. This approach enhances the photocurrent of the cell without deterioration of its electrical characteristics, it is fully compatible with many thin film manufacturing processes such as roll-to-roll[18] and involves low processing temperatures (below 200 °C).

Photonic electrodes were fabricated by soft nanoimprinting a photoresist film using a pre-patterned PDMS (Polydimethylsiloxane) mold, followed by ITO sputtering. Nanoimprinting lithography allows the inexpensive and multiple replication of a pattern engraved (typically by electron beam lithography) on a silicon wafer (master) onto different surfaces.[24,25] This technique yields a great variety of photonic structures such as the ones used herein or the plasmonic crystals obtained after metal coating an imprinted surface.[26] Nanoimprinted photonic structures have been incorporated in solar devices in the form of plasmonic scattering layers in amorphous silicon solar cells[27] or as 2D gratings in silicon microcells.[28] To the best of our knowledge, very little work has been done combining solution processed solar cells and soft imprinting. The use of a rigid stamp to produce patterned organic solar cells (PCDTBT/PC70BM) has been reported, but no in-depth analysis of the optical properties of the final structures was provided.[29] A typical patterning process starts with imprinting a UV curable photoresist (or a sol gel) deposited onto the silicon active layer. Then, several etching processes are performed to transfer the pattern into the semiconductor substrate, to finally remove the resist.[30] Our approach does not require any kind of etching for the imprinted thermally stable epoxy is left as part of the final device, reducing the number of processing steps that could affect the electrical performance of the active layer. Despite the simplistic fabrication procedure, the resulting photonic architectures exhibit strong diffraction which greatly improves the performance of the solar cells and can be easily implemented in other optoelectronic devices. **Figure 1** illustrates the fabrication flow of the imprinted structures and assembly of the

Dr. A. Mihi, Dr. F. J. Beck, Dr. T. Lasanta,
Dr. A. K. Rath, Prof. G. Konstantatos
Prof. Gerasimos Konstantatos, Dr. Agustín Mihi
ICFO-Institut de Ciencies Fotoniques
Mediterranean Technology Park
08860 Castelldefels, Barcelona, Spain
E-mail: gerasimos.konstantatos@icfo.es

DOI: 10.1002/adma.201303674

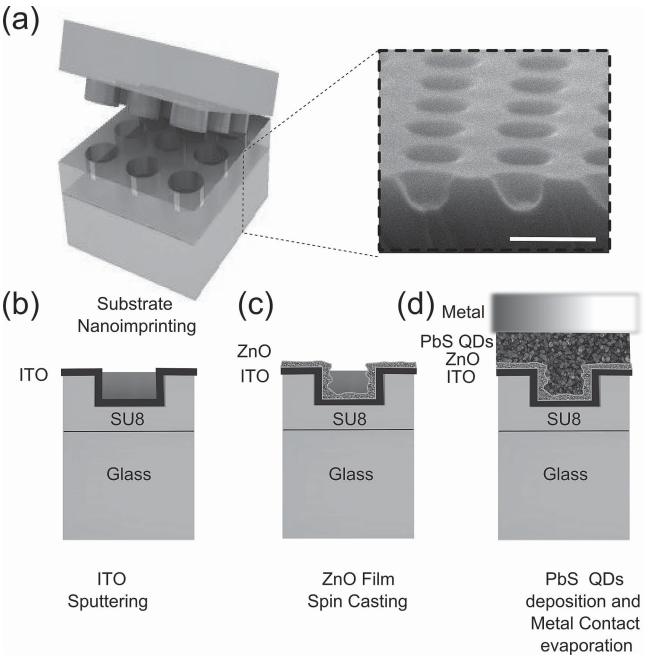

Figure 1. Schematized fabrication flow of the PbS-ZnO solution processed solar cell on an ITO coated imprinted substrate. A soft imprinted epoxy (a) is coated with 40 nm of ITO by sputtering deposition (b). Next, the heterojunction solar cell is built onto the imprinted electrodes by (c) spin casting and sintering ZnO nanocrystals and (d) the layer-by-layer deposition of the PbS quantum dots crosslinked with MPA (3-Mercapto propionic acid), finishing with the evaporation of the metal contacts. The inset displays a cross-sectional SEM image (45° angle) of an imprinted photoresist surface, the scale bar is 500 nm.

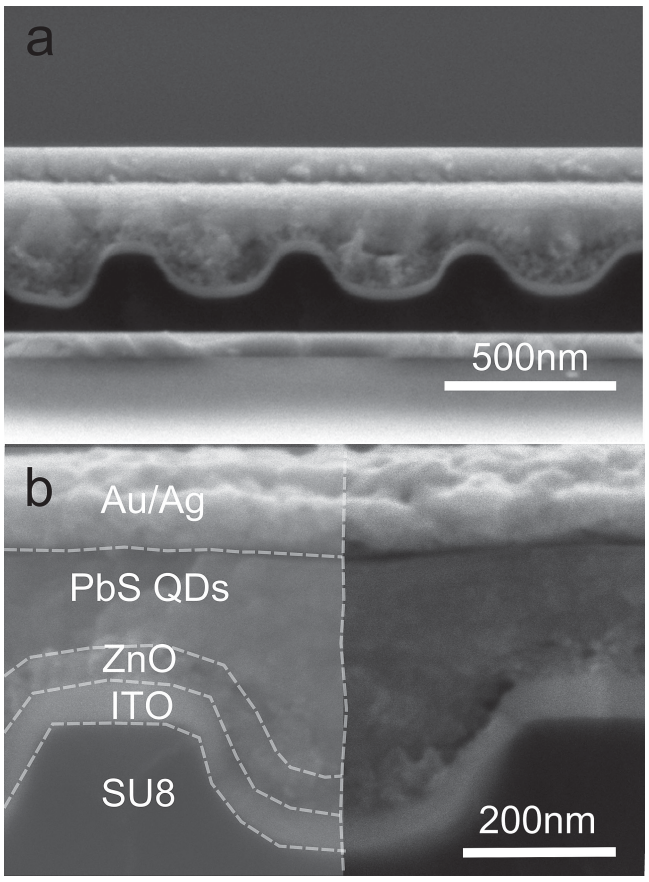

Figure 2. (a) Scanning electron micrograph of a PbS-ZnO heterojunction solar cell on an imprinted electrode (L = 550 nm and r = 200 nm) and (b) zoomed in view where the different components of the cells can be distinguished. From top to bottom: the metal electrode (15 nm of MoO_3, 40 nm of Au and 100 nm of Ag), 200–240 nm thick film of PbS quantum dots, 60–80 nm of ZnO nanocrystals and 40 nm of sputtered ITO on the imprinted SU8 resist.

PbS-ZnO heterojunction solar cell (see Experimental Section for details). Figure 1a represents the nanoimprinting process of a 300 nm thick photoresist (SU8, Microchem) coated substrate. The inset in Figure 1 displays an SEM image of the square array patterned epoxy after imprinting. The resist is UV cured to improve its mechanical stability, and coated with 40 nm of ITO (Figure 1b). The PbS-ZnO bilayer is then fabricated on the imprinted electrodes by spin casting 80 nm of ZnO nanocrystals (Figure 1c) and 200 nm of PbS colloidal quantum dots. The quantum dots are deposited in a layer by layer fashion, each followed by a ligand exchange step performed while spinning, as described elsewhere.[19] Each cycle forms a 20 nm quantum dot layer that follows the corrugation of the substrate at first, but becomes flat after 5 deposition cycles and is completely planar by the time the thickness of the optimized device reaches 200 nm. The device is completed with the evaporation of metallic contacts (Figure 1d). A cross-sectional SEM image from the resulting solar cell can be found in **Figure 2**a, together with a closer view of the different layers composing a unit cell of the square array (Figure 2b). Throughout the fabrication process of the solar cell, the films are annealed at 200 °C twice, first after the ITO sputtering to improve conductivity and second, to sinter the ZnO nanocrystalline film after spin casting. The SU8 epoxy is quite stable at these temperatures as is intended to form part of the final device once hard baked at 150 °C.

The final configuration of our cells consists of a 2D periodic array structure on the front of the cell (light impinging from the glass/SU8) and flat mirror (back electrode) in the back. The intention of this architecture is to have a diffractive element on the front and a back reflector, an optimum configuration for light trapping, as predicted theoretically for thin solar cells.[31]

The imprinted electrode was designed to maximize the light harvesting efficiency of the PbS QD-ZnO heterojunction in the near infrared where the quantum dots exhibit the first excitonic peak. To do so, the wavelength dependent absorption enhancement (**Figure 3**a) was computed with FDTD (Finite Differences Time Domain) for different lattice parameters (L) of a square array of cylinders (radious, r = 220 nm) coated with 40 nm of ITO, 80 nm of ZnO and 200 nm of PbS layers (parameters that yielded the best results in the flat electrode device). According to these calculations, the optimum lattice parameter to enhance light harvesting at the wavelength of 1 μm would be 550 nm. From this graph, it can be inferred how the absorption enhancement depends on the lattice parameter of the array indicating that it is originated by diffraction from the square lattice, unlike other resonant modes of the geometry.[32] The diffracted light is coupled to trapped modes propagating within the cell, increasing its absorption. The influence of

Adv. Mater. 2013,
DOI: 10.1002/adma.201303674

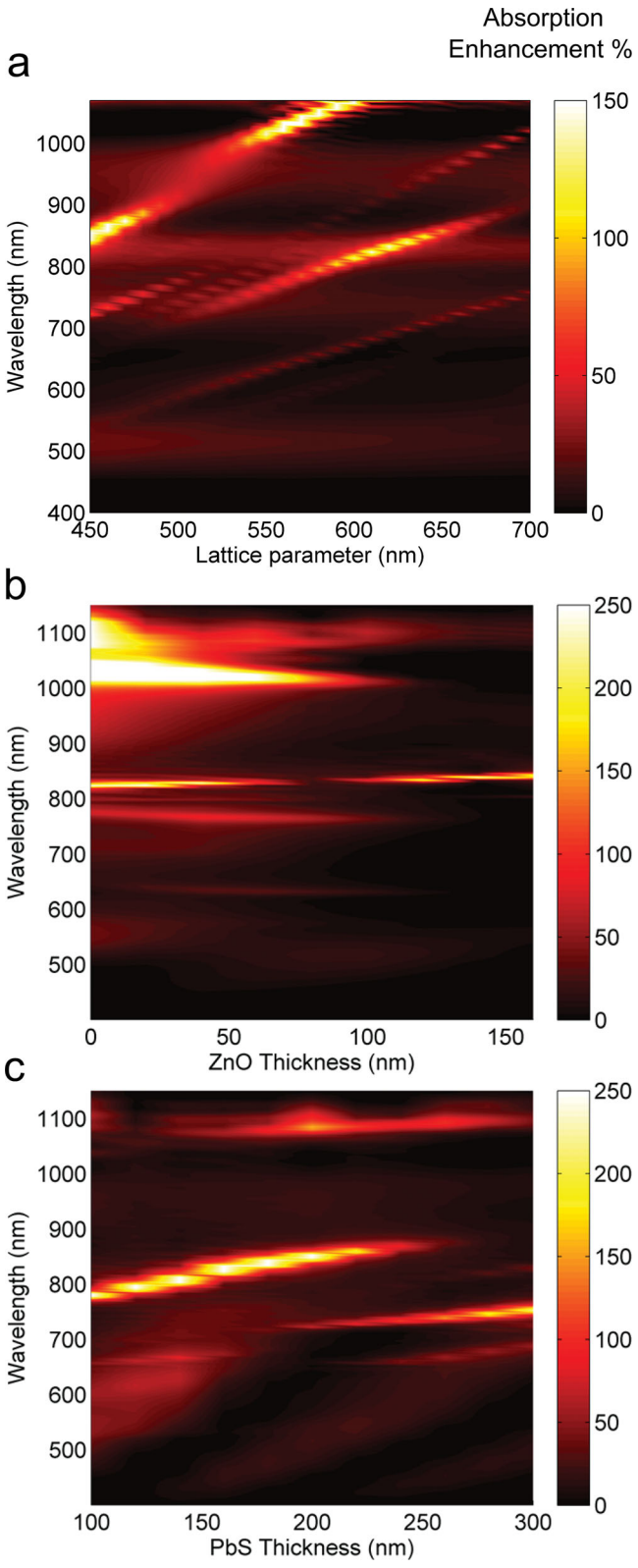

Figure 3. Simulated absorption enhancement (%) of a PbS QDs-ZnO heterojunction built on an imprinted versus a flat electrode with varying (a) lattice parameter,(b) ZnO layer and (c) PbS layer thicknesses. Unaltered parameters were fixed to r (220 nm), L (550 nm), ITO (40 nm), ZnO (80 nm), PbS (200 nm).

both PbS and ZnO layers is also taken into account and represented in Figure 3b and 3c. Those calculations indicate that the maximum enhancement would be attained without a ZnO layer, attributed to a stronger diffraction of the structure due to a corrugated high refractive index material (n_{PbS} = 2.4 vs $n_{nc\text{-}ZnO}$ = 1.7). It should be also noted that the array would produce intense enhanced absorption for other wavelengths (850 nm) even at thicker ZnO layers, for the selected lattice parameter of 550 nm. Experimentally, the ZnO layer acts as the electron acceptor for the PbS quantum dot film and therefore, necessary for a high efficiency cell. Nevertheless, this result indicates that our electrodes would be even more beneficial to other solar cell architectures such as bulk heterojunctions that do not require the presence of the oxide layer.[33] The thinnest oxide layer experimentally achieved was 80 nm as thinner films led to shorted devices. In the case of the PbS layer, as the thickness is increased additional wavelength dependent enhancement is seen at short wavelengths, and red-shifts. This is due to the fact that there is a larger number of trapped modes supported by the PbS as it gets thicker, and is indicative that we are facilitating diffractive coupling to these modes. The PbS thickness (200 nm) was chosen considering the optical design and the electrical constraints imposed by the carrier diffusion lengths (200–250 nm) in these films.

The measured external quantum efficiency spectra (EQE) of the devices made on flat and imprinted electrodes are plotted in **Figure 4**a next to the simulated absorption for comparison (Figure 4b). The continuous and dashed lines correspond in each case to the imprinted array and the flat reference cells. A clear enhancement can be seen at wavelengths close to the characteristic excitonic peak of the PbS quantum dots (1055 nm). The magnitude of the enhancement in EQE (red dotted line in Figure 4a) correlates very well to the enhancement in simulated absorption (red dotted line in Figure 4b). The imprinted cell exhibits enhanced spectral response for wavelengths ranging from 600 nm up to 1100 nm reaching values up to 100% (over 120% in simulation) with respect to the flat device at the excitonic peak of the PbS quantum dots.

The explanation to the enhanced absorption in the imprinted electrodes can be found in the spatial distribution of the electric field intensity, shown in Figure 4c-d for the three wavelengths indicated in Figure 4b as λ1, λ2 and λ3. The white arrow indicates the direction of incidence of the incoming illumination, while the white dashed lines surround the region where the absorbing PbS quantum dots are located and indicate the glass/resist interface. The simulated mode profiles show high field intensity regions confined at the higher refractive index quantum dot layer (n = 2.4), which facilitates the absorption of light in the active layer (λ2 and λ3) and to a lesser extent in (λ1), where intense electric field can also be found within the non-absorbing ZnO/ resist layer. From these simulations it can be concluded that when light impinges on a solar cell built on an imprinted electrode, is diffracted into modes propagating mainly within the thickness of the imprinted solar cell boosting the absorption of light.

Finally, current – voltage characteristics for the devices are presented in **Figure 5**, the extracted figures of merit summarized in the inset. The enhanced absorption exhibited by the imprinted electrode results in a higher photocurrent (17.5% higher) than

ADVANCED MATERIALS
www.advmat.de

www.MaterialsViews.com

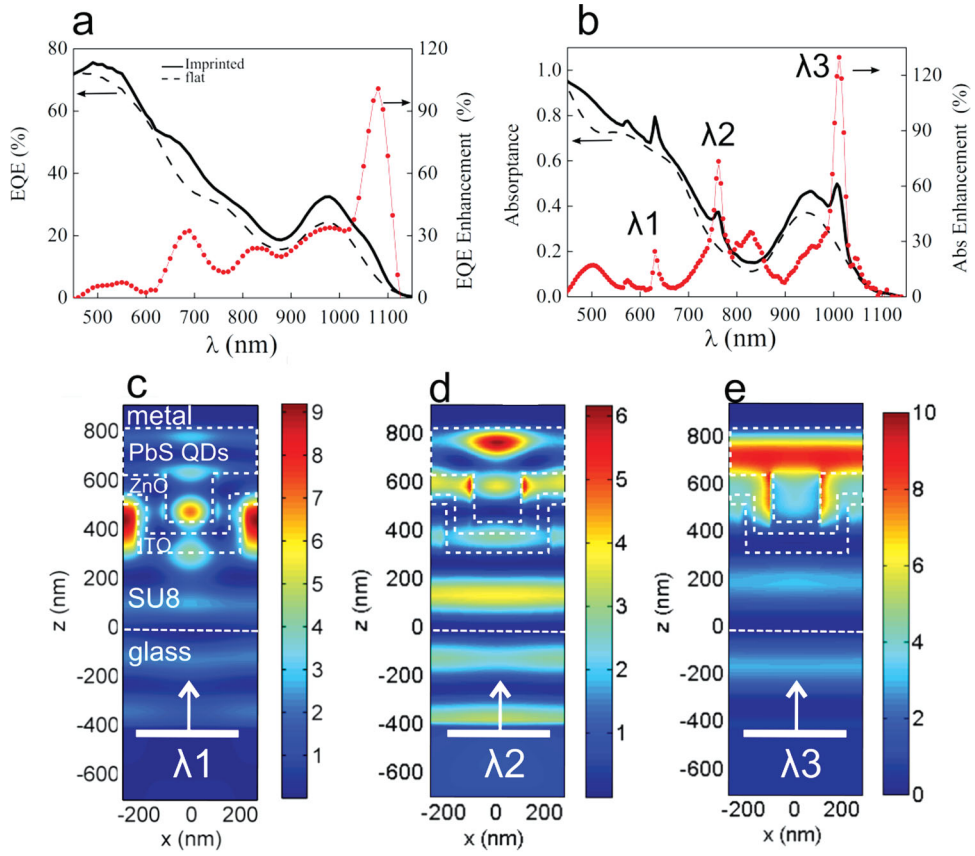

Figure 4. (a) External quantum efficiency (EQE) data measured from an imprinted cell (black line) and a flat reference cell (dashed line).The enhancement in EQE (%) is included in the right axis (red dotted line). (b) FDTD Simulated absorptance spectra for a square array (L = 550 nm, r = 220 nm) based cell (black line) and flat reference cell (dashed line). In all cases the resist, ITO and ZnO thicknesses were fixed at 300, 40, 80 and 200 nm respectively, according to the values measured from the SEM cross-sections of the actual devices. The enhancement in absorption (%) is included in the right axis (red dotted line). λ1, λ2 and λ3 represent the three wavelengths for which the spatial distribution of the electric field has been calculated (color bar) in (c–e). Indicated in each field distribution graph is the direction of incidence of the light, the location of the glass/resist interface and the PbS area for a single unit cell of the 2D array.

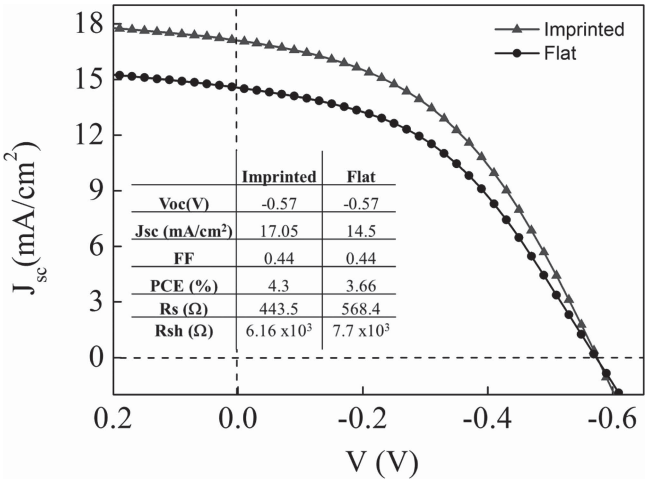

Figure 5. *I–V* characteristics for the champion imprinted (triangles) and flat (dots) devices. The different figures of merit extracted from these curves are presented in the inset table. Open circuit Voltage (V_{oc}), short-circuit Current Density (J_{sc}), fill factor (FF), Power Conversion Efficiency (η) and series and shunt resistivity (R_s and R_{sh}).

the flat reference cell. Interestingly, the corrugation of the structure causes minimal deterioration of the electrical characteristics of the cell, since both reference cell and the imprinted electrode perform similarly in terms of fill factor (FF) and open circuit voltage (Voc) and therefore, the enhancement in photocurrent is directly reflected in a 17.5% enhancement in power conversion efficiency from 3.7% to 4.3% (more results from different devices are presented in Figure S1, Supporting Information).

In conclusion, we have fabricated imprinted electrodes that improve the photocurrent of solution processed solar cells using a low cost and low temperature approach. The power conversion efficiency of an imprinted cell was enhanced with respect to the flat case by confining light within the thickness of the imprinted solar cell. The 17.5% enhancement in photocurrent results in a 17.5% enhancement in efficiency of the cell, from 3.7% to 4.3%, since no electrical parameters of the cell were deteriorated by the corrugation. The method presented herein, relies on the patterning of a common component in many thin film solar cells; the TCO, and therefore it would be straightforward to implement in other technologies. We believe that this architecture offers new possibilities in the fabrication

DOI: 10.1002/adma.201303674

of wave optics based light trapping schemes for emerging technologies with sub-micron active layers and will allow the fabrication of many interesting architectures modeled in the literature,[34] while maintaining the ease of manufacture and low costs that made these new technologies so appealing.

Experimental Section

Nanostructured electrodes were fabricated by nanoimprinting on an ethanol wetted 300 nm film of UV photo curable epoxy (SU8, Microchem) spin casted on an ITO coated substrate. A poly(dimethylsiloxane) mold (PDMS, 10:1 Sylgard 184) replicating a square array pattern from a silicon wafer (AMO gratings) was used as "printing stamp". The resist is UV cured (λ = 360 nm, 15 min) through a spatial mask defining squared imprinted regions of 9 mm^2. After exposure and development of the resist, 4 squared regions of imprinted resist are left. 40 nm of ITO are sputtered on the substrates using an AJA sputtering system without masking so the sputtered ITO is electrically connected to a commercial ITO coated substrate. Finally a 90 min anneal at 200°C under inert atmosphere is carried out to improve the conductivity of ITO (see supporting information).

Flat electrodes were prepared by sputtering ITO on cleaned commercial ITO substrates, so the electrode over which the ZnO-PbS QDs heterojunctions were deposited would have the same work function.

Halide Treated Lead sulfide Nanocrystals with 940 nm excitonic peak were synthesized following a modified recipe from the literature.[35] Cadmium chloride treatment of the PbS quantum dots took place after addition of the sulfur source during the cooling process by injecting 0.5 mL of a solution of $CdCl_2$ (0.65 mmol), TDPA (0.05 mmol) and oleylamine (2 mL) previously prepared at 100 °C under vacuum for 16 h.[19] The nanocrystals were isolated by the addition of 5 mL of toluene and 24 mL absolute ethanol followed by centrifugation, then purified by dispersion/precipitation with toluene/ethanol three or four more times before final dispersal in anhydrous toluene (40 mg mL^{-1}).

Zinc Oxide films were spin casted at 2500 r.p.m. from a ZnO nanocrystal dispersion in chloroform followed by annealing at 200 °C for 30 min as described in the literature.[36]

PbS-ZnO bilayers solar cells were fabricated by the alternate spin casting of PbS nanocrystals in toluene (40 mg mL^{-1}) and MPA (3-Mercapto propionic Acid, 2% in Methanol) at 3000 r.p.m. followed by a methanol rinse. Each step produced layers of 20 nm thick films. The process was repeated 10 times to achieve the desired thickness of 200 nm. Finally, 15 nm MoO_3, 40 nm Au and 120 nm of Ag were thermally evaporated on top (Lesker evaporator).

Current-voltage characteristics were obtained using a Keithley 2400 source measuring unit under dark and simulated AM1.5 solar conditions (Oriel Sol3A, class AAA). External quantum efficiency (EQE) measurements were obtained using a Newport Cornerstone 260 monochromator and a Keithley 2400 source measuring unit providing short-circuit conditions.

Optical simulations were carried out using a commercial fully vectorial FDTD simulation package Lumerical (www.lumerical.com). The calculations were performed in a single unit cell with periodic boundary conditions in the xy-plane and perfectly matched layer boundary conditions in the z plane (see Figure 3 e-g). The fields within the PbS were monitored and the absorption of the metal contacts discriminated. The refractive indexes of the resist, ITO and nanocrystalline ZnO were considered constant at 1.6, 1.9 and 1.7 for simplicity. A wavelength dependent complex refractive index of PbS was calculated from transmittance spectra, as described elsewhere.[37]

Supporting Information

Statistical variation of the figures of merit from the devices presented, ITO electrical and optical characteristics and transmittance and reflectance measurements of flat, imprinted and rough electrodes for comparison. Supporting Information is available from the Wiley Online Library or from the author.

Acknowledgements

We acknowledge financial support from Fundació Privada Cellex Barcelona and Ministerio de Ciencia e Innovación under contract number TEC2011–24744. We also acknowledge support from the Nanophotonics for Energy Network of Excellence under contract N4E GA.248855. A.M. was supported by an ICFONEST (COFUND program) postdoctoral fellowship. F.J.B. acknowledges the support of a Marie Curie postdoctoral fellowship (PECQDPV, FP7-people-2011-IIF).

Received: August 7, 2013
Revised: September 14, 2013
Published online:

[1] R. R. Lunt, T. P. Osedach, P. R. Brown, J. A. Rowehl, V. Bulović, *Adv. Mater.* **2011**, *23*, 5712–27.
[2] I. J. Kramer, E. H. Sargent, *ACS nano* **2011**, *5*, 8506–14.
[3] S. R. Forrest, *Nature* **2004**, *428*, 911–8.
[4] C. J. Brabec, N. S. Sariciftci, J. C. Hummelen, *Adv. Funct. Mater.* **2001**, *11*, 15–26.
[5] F. C. Krebs, *Sol. Energ. Mat. Sol. Cells* **2009**, *93*, 394–412.
[6] H. W. Deckman, *Appl. Phys. Lett.* **1983**, *42*, 968.
[7] Z. Yu, A. Raman, S. Fan, *Proc. Natl. Acad. Sci. USA* **2010**, *107*, 17491–6.
[8] C. Battaglia, C.-M. Hsu, K. Söderström, J. Escarré, F.-J. Haug, M. Charrière, M. Boccard, M. Despeisse, D. T. L. Alexander, M. Cantoni, Y. Cui, C. Ballif, *ACS nano* **2012**, *6*, 2790–7.
[9] D. M. Callahan, J. N. Munday, H. A. Atwater, *Nano Lett.* **2012**, *12*, 214–8.
[10] A. Polman, H. A. Atwater, *Nat. Mater.* **2012**, *11*, 174–7.
[11] V. K. Narasimhan, Y. Cui, *Nanophotonics* **2013**, *2*, 187–210.
[12] K. A. Arpin, A. Mihi, H. T. Johnson, A. J. Baca, J. A. Rogers, J. A. Lewis, P. V Braun, *Adv. Mater.* **2010**, *22*, 1084–101.
[13] K. R. Catchpole, M. A. Green, *J. Appl. Phys.* **2007**, *101*, 063105.
[14] Y. Park, E. Drouard, O. El Daif, X. Letartre, P. Viktorovitch, A. Fave, A. Kaminski, M. Lemiti, C. Seassal, *Opt. Express* **2009**, *17*, 14312.
[15] A. Chutinan, N. P. Kherani, S. Zukotynski, *Opt. Express* **2009**, *17*, 8871.
[16] P. Bermel, C. Luo, L. Zeng, L. C. Kimerling, J. D. Joannopoulos, *Opt. Express* **2007**, *15*, 16986.
[17] C. Heine, R. H. Morf, *Appl.Optics* **1995**, *34*, 2476–82.
[18] S. H. Ahn, L. J. Guo, *ACS nano* **2009**, *3*, 2304–10.
[19] A. H. Ip, S. M. Thon, S. Hoogland, O. Voznyy, D. Zhitomirsky, R. Debnath, L. Levina, L. R. Rollny, G. H. Carey, A. Fischer, K. W. Kemp, I. J. Kramer, Z. Ning, A. J. Labelle, K. W. Chou, A. Amassian, E. H. Sargent, *Nat. Nanotech.* **2012**, *7*, 577–82.
[20] A. G. Pattantyus-Abraham, I. J. Kramer, A. R. Barkhouse, X. Wang, G. Konstantatos, R. Debnath, L. Levina, I. Raabe, M. K. Nazeeruddin, M. Grätzel, E. H. Sargent, *ACS nano* **2010**, *4*, 3374–80.
[21] P. R. Brown, R. R. Lunt, N. Zhao, T. P. Osedach, D. D. Wanger, L.-Y. Chang, M. G. Bawendi, V. Bulovi , *Nano Lett.* **2011**, *11*, 2955–61.
[22] J. Gao, C. L. Perkins, J. M. Luther, M. C. Hanna, H.-Y. Chen, O. E. Semonin, A. J. Nozik, R. J. Ellingson, M. C. Beard, *Nano Lett.* **2011**, *11*, 3263–6.
[23] J. Jean, S. Chang, P. R. Brown, J. J. Cheng, P. H. Rekemeyer, M. G. Bawendi, S. Gradečak, V. Bulović, *Adv. Mater.* **2013**, *25*, 2790–6.
[24] S. Y. Chou, P. R. Krauss, P. J. Renstrom, **1996**, *14*, 4129–4133.

[25] Y. Xia, J. A. Rogers, K. E. Paul, G. M. Whitesides, *Chem. Rev.* **1999**, *99*, 1823–1848.
[26] D. Chanda, K. Shigeta, T. Truong, E. Lui, A. Mihi, M. Schulmerich, P. V Braun, R. Bhargava, J. A. Rogers, *Nat. Comm.* **2011**, *2*, 479.
[27] V. E. Ferry, M. A. Verschuuren, H. B. T. Li, R. E. I. Schropp, H. A. Atwater, A. Polman, *Appl. Phys. Lett.* **2009**, *95*, 183503.
[28] D. Shir, J. Yoon, D. Chanda, J.-H. Ryu, J. A. Rogers, *Nano Lett.* **2010**, *10*, 3041–6.
[29] D. H. Wang, J. Seifter, J. H. Park, D.-G. Choi, A. J. Heeger, *Adv. Energy Mater.* **2012**, *2*, 1282–1282.
[30] H. Hauser, B. Michl, S. Schwarzkopf, V. Kübler, C. Müller, M. Hermle, B. Bläsi, *IEEE J. Photovoltaics* **2012**, *2*, 114–122.
[31] A. Raman, Z. Yu, S. Fan, *Opt. Express* **2011**, *19*, 19015–26.
[32] A. P. Vasudev, J. A. Schuller, M. L. Brongersma, *Opt. Express* **2012**, *20*, A385.
[33] A. K. Rath, M. Bernechea, L. Martinez, F. P. G. de Arquer, J. Osmond, G. Konstantatos, *Nat. Photonics* **2012**, *6*, 529–534.
[34] M. G. Deceglie, V. E. Ferry, A. P. Alivisatos, H. A. Atwater, *Nano Lett.* **2012**, *12*, 2894–900.
[35] M. a. Hines, G. D. Scholes, *Adv. Mater.* **2003**, *15*, 1844–1849.
[36] J. M. Luther, J. Gao, M. T. Lloyd, O. E. Semonin, M. C. Beard, A. J. Nozik, *Adv. Mater.* **2010**, *22*, 3704–7.
[37] F. P. García de Arquer, F. J. Beck, G. Konstantatos, *Opt. Express* **2011**, *19*, 21038–49.

Adv. Mater. **2013**,
DOI: 10.1002/adma.201303674